

## Article

# Fractional Frequency Reuse Optimal SINR Threshold Selection Using NIR and ISODATA

Peter Kihato, Stephen Musyoki and Antony Onim \*

Department of Electrical and Electronic Engineering, Institute of Basic Sciences and Technology Innovation, Pan African University, Nairobi 35525-00100, Kenya; pkihato@kuat.ac.ke (P.K.); smusyoki@yahoo.com (S.M.)  
\* Correspondence: onim.antony@gmail.com; Tel.: +254-721-148-180

**Abstract:** A vital part of cellular network evolution has been long-term evolution networks. In these networks, it is important to mitigate inter-cell interference. Fractional frequency re-use has been proposed to address this. The method involves the division of cells into two regions based on a signal-to-interference-plus-noise-ratio threshold value. The inner region adopts a frequency re-use of one (1), while the outer region uses a higher frequency re-use factor. Setting the threshold value is a critical problem addressed in this paper. The proposed approach adapts techniques used in image processing called global-thresholding techniques. The approaches considered are iterative self-organizing data analysis and native integral ratio. Mobile stations in a cell continuously report their signal-to-interference-plus-noise-ratio values to the base station. These reported values are used to determine a threshold which dictates which subscribers fall in the inner and outer regions. The threshold value is periodically updated based on the new reported values over time. Simulations are used to assess the performance using throughput and fairness metrics. By setting the threshold optimally, better throughputs and fairness are then achieved. We concluded that native integral ratio marginally outperformed the iterative self-organizing data analysis method, and it significantly outperformed static fractional frequency reuse techniques.



**Citation:** Kihato, P.; Musyoki, S.; Onim, A. Fractional Frequency Reuse Optimal SINR Threshold Selection Using NIR and ISODATA. *Telecom* **2022**, *3*, 433–447. <https://doi.org/10.3390/telecom3030023>

Academic Editor: Achilles D. Boursianis

Received: 13 June 2022

Accepted: 1 July 2022

Published: 7 July 2022

**Publisher's Note:** MDPI stays neutral with regard to jurisdictional claims in published maps and institutional affiliations.



**Copyright:** © 2022 by the authors. Licensee MDPI, Basel, Switzerland. This article is an open access article distributed under the terms and conditions of the Creative Commons Attribution (CC BY) license (<https://creativecommons.org/licenses/by/4.0/>).

**Keywords:** fractional frequency reuse; native integral ratio; throughput; fairness; iterative self organizing data analysis

## 1. Introduction

Orthogonal frequency division multiple access (OFDMA) is a long-term evolution technology (LTE). OFDMA has been used in cellular networks to effectively reduce intra-cell interference [1,2]. Fractional frequency re-use (FFR) in LTE networks works by splitting the cell frequencies into two regions: the outer and the inner regions. The outer region adopts a higher re-use factor. Typically, a re-use factor of three (3) is commonly used. This way the frequencies used in the outer region are re-used in alternate cells, hence reducing cell interference. The inner region uses a more aggressive frequency re-use factor, hence improving throughput. Signal-to-interference-plus-noise-ratio (SINR) threshold is a very important parameter in FFR schemes. It dictates which regions the subscribers in a cell will fall [3]. The problem of setting the SINR threshold to achieve optimal throughput and fairness are addressed in this paper. This paper also addresses the gap in earlier articles where the SINR threshold was not continuously updated over time. This is vital since the cell dynamics keep changing with subscriber movement. There is, therefore, a need to periodically update the SINR threshold. Some earlier publications also failed to consider fairness as a performance metric. Throughput alone is not sufficient to measure network performance. A network can have high throughput which is only concentrated among a few subscribers with good SINR. Fairness ensures that even subscribers with poor SINR are also considered during frequency allocation. Image-processing techniques use thresholding of pixel values as a means of distinguishing between the background and foreground [4–6].

This popular technique is referred to as global thresholding since a single threshold value is set for the entire image [7]. Global thresholding is desirable for our study since we need to set a single SINR threshold. We adapted pixel values as an input and replaced them with SINR values reported in the cell. The selected threshold value separates the outer and inner region subscribers. Our work considered two methods, i.e., iterative self-organizing data analysis (ISODATA) and native integral ratio (NIR). NIR has been utilized in setting a threshold in handwritten documents that were used for forensic purposes. The pixels forming the handwriting gets categorized into classes of three, i.e., fuzzy, foreground, and background. In between the background and the foreground sits the fuzzy class. The fuzzy pixels are not definitively defined where they exactly fall [8]. ISODATA on the other hand has been used by eye specialists in diagnosing diabetic retinopathy. The process involves segmentation of retinal images of the eye and dividing them into retinal background and blood vessels [9]. Edge throughput and fairness are the performance parameters used to measure the effectiveness of the approaches considered. Poor SINR values are mostly found near the cell edge, and such subscribers tend to suffer dismal throughput. It is important to incorporate fairness as throughput alone can be very misleading. A cellular network might have high throughput; however, the throughput is exclusively enjoyed by just a few subscribers with good SINR values.

Various frequency allocation schemes have been used widely such as: best channel quality indicator (CQI), proportionally fair (PF), and round robin (RR). Our paper adopted PF scheduler as it forms a great balance between throughput and fairness metric. Round robin would have offered improved fairness. However, equal allocation of resources to subscribers even with poor SINR means that network throughput is reduced. On the other hand, best CQI prioritizes frequency allocation based on signal strength. Only subscribers with the best signal would get the frequency resources at the expense of those with poor signals. This would lead to higher network throughputs but poor fairness.

The main contribution of this paper is in setting an optimal SINR threshold which is periodically updated. This would yield better throughputs and fairness. The approaches considered were ISODATA and NIR and were compared with static FFR. NIR was found to perform best by achieving better throughput and fairness.

## 2. Literature Review

### 2.1. Cellular Network Model

The base station (BS) positioned at the center of each hexagon represents the area of coverage, as depicted in Figure 1 below. A circle with identical radius  $r = (\sqrt{3\sqrt{3}/2\pi})H_s$ ,  $H_s$  is the side of the hexagon. The resulting area of coverage total is  $A_T^c = \pi(r^2 - r_0^2)$ . The shortest distance between the nearest mobile station (MS) to the serving base station is  $r_0$ .

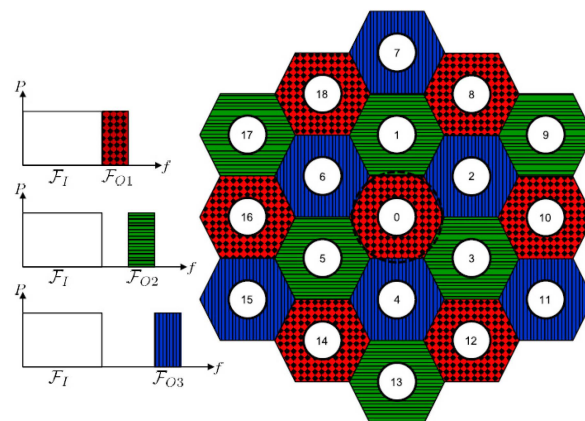


Figure 1. Two-layer FFR network layout.

### 2.2. FFR Network Layout

Standard FFR architecture is split into the outer region, also referred to as partial re-use zone, and the inner region, popularly referred to as full re-use zone [10]. The received SINR values from the subscribers dictates how the threshold is set and which subscribers fall in the respective regions. In the event the received SINR value is higher than the threshold denoted as  $\Gamma_{th}$ , the subscriber is then categorized in the inner region. If not, it is regarded to be in the outer region or the partial-reuse zone. The inner and outer regions are allocated disjoint frequencies.  $B_T$ , which is the total system bandwidth and contains orthogonal subcarriers,  $R_T$  and  $B_T$ , is divided into  $B_I$ , which is a cluster of subcarriers in the inner region. Sub-carrier cluster,  $B_O = B_T \setminus B_I$ , is allocated to outer region subscribers.  $B_O$  cluster is again split into three parts,  $B_{O1}$ ,  $B_{O2}$ , and  $B_{O3}$  [10]. The three parts allocated to the MSs in the outer cell ensure every adjacent cell is operating at different sub-band frequencies.

Hence,

$$R_T = 3R_O + R_I \tag{1}$$

Inner region and outer regions are respectively assigned subcarriers,  $R_I$  and  $R_O$ .

$\beta_{FR}$  is the ratio of subcarrier numbers that fall in the inner region. The outer region gets allocated,  $1 - \beta_{FR}$ , of all the available system bandwidth.

### 2.3. SINR

Considering path loss,  $N_{dB}$ , and small-scale fading as in [11], the modelling of the channels that links MS  $d$  and BS  $p$  can be obtained as:

$$N_{dB}(C_{d,p}) = \log_{10}(C_{d,p})10\alpha + K \tag{2}$$

$K$  is a constant representing path loss at a meter from the BS, and  $\alpha$  represents the pathloss exponent that varies depending on the environment of operation. Distance between MS  $d$  and BS  $p$  is  $C_{d,p}$  which is measured in meters.

$Z$  represent cell layers,  $O$  or  $I$ , having MS  $b$  located in the cell served by a BS  $p$ . During the scheduling period,  $t$ , the  $n$ th subcarrier instantaneous SINR  $W_{p,l}^Z(t)$ , is obtained by:

$$W_{p,l}^Z(t) = \frac{|D_{d,p,l}(t)|^2 P_w G_T N(c_{0,p})}{I_{p,l}^Z(t) + N_0 F_n \Delta b} \tag{3}$$

The BS antenna gain is represented by  $G_T$ , whereas  $P_w$  is the power assigned to each subcarrier.  $N(c_{0,p})$  represents the path loss. The frequency response due to small-scale fading is  $D_{d,p,l}(t) \sim JN(0,1)$  within the channel that connects MS  $u$  and BS  $b$  during scheduling period,  $t$ , on the  $n$ th subcarrier. The power spectral noise density (PSD) is  $N_0$ , and the noise factor is represented by  $F_n$ .  $\Delta b$  represents the subcarrier frequency bandwidth. The interference term  $I_{p,l}^Z(t)$  is given by:

$$I_{p,l}^Z(t) = \sum_{d \in \Phi_l^Z} P_w G_T N(c_{d,p}) |D_{d,p,l}(t)|^2 \tag{4}$$

where  $N(c_{d,p})$  represents the path loss, and  $D_{d,p,l}(t)$  represents the small-scale fading. The set of interfering BSs that depend on the FFR layer of subcarrier and the subcarrier itself is represented by  $\Phi_n^Z$ . Figure 1 shows the interfering base station set as follows:

$$\Phi_l^Z = \begin{cases} \{1, 2, \dots, 18\}, & l \in B_I \\ \{8, 10, 12, 14, 16, 18\}, & l \in B_O \end{cases} \tag{5}$$

If we assume a homogeneous power allocation, then each subcarrier power allocation is

$$P_w = \frac{P_T}{R_I + R_O} \quad (6)$$

$P_T$  represents the available power at the BS transmitter.

#### 2.4. Throughput

Downlink throughput is directly affected by SINR of a channel of every MS as illustrated by Shannon- Hartley theorem [12].

$$C = \log_2 \left( W_{p,l}^Z(t) + 1 \right) B_T \quad (7)$$

where  $C$  connotes the capacity of the channel in bits/s.

#### 2.5. Jain's Index of Fairness

A more comprehensive FFR scheme performance evaluation is accomplished by considering both fairness and throughput [13]. Jain's fairness index is important as it grades how throughput is equitably distributed among subscribers. Jain's fairness index is expressed as:

$$J(x) = \frac{\left( \sum_{i=1}^N x_i \right)^2}{N \sum_{i=1}^N x_i^2} \quad (8)$$

The number of users in each coverage areas is denoted by  $N$ , while the throughput that the  $i$ th user experiences is given by area of coverage  $x_i$ .

#### 2.6. Proportionally Fair (PF) Scheduling

PF scheduling is a channel-aware-scheduling technique which aims to strike a balance between ensuring throughput and fairness [14]. The prioritization coefficient is  $P_c(t)$  where  $P_c(t) = 1/\mu_p(t)$  is given to every MS based on their anticipated resource consumption. The channel-state information short-term average evolution is  $\mu_p(t)$ . It is obtained using the moving average over a window  $W$ .

$$\mu_p(t) = \mu_p(t-1) \left( 1 - \frac{1}{W} \right) + \sum_{l \in B_Z} \iota_{p,l}(t) \frac{W_{p,l}^Z(t)}{W} \quad (9)$$

$\iota_{p,l}(t)$  shows if MS  $q$  in scheduling period  $t$  during  $n$ th subcarrier can communicate, i.e.,

$$\iota_{q,n}(t) = \begin{cases} 1, & \text{when MS } p \text{ is scheduled on carrier } l \text{ in } t \\ 0, & \text{else} \end{cases} \quad (10)$$

Instantaneous SINR information is exploited by the PF scheduler which is experienced by all MSs  $q \in \mathcal{M}_A$  and allocates subcarrier  $l \in \mathcal{F}_A$  to MS  $u \in \mathcal{M}_A$ , satisfy the condition:

$$u = \arg \max_{q \in \mathcal{M}_A} \left\{ P_c(t) W_{p,l}^Z(t) \right\} \quad (11)$$

$\mathcal{M}_A$  represents the total MSs number in a certain cell area,  $A$ .

#### 2.7. Native Integral Ratio (NIR) Method

Typically, global thresholding is done in one stage where the image pixels are separated into foreground and background. Global threshold methods target to achieve a specific threshold value to do the separation [8]. NIR thresholding aims to add a third category of pixels called fuzzy class. In the fuzzy class it is not clear whether these pixels fall in the foreground or background [8,15]. Two critical values,  $M$  and  $N$ , are, therefore,

determined. The foreground and fuzzy class boundary, and the background and fuzzy class boundary, exist respectively. The technique first determines these two boundaries then later determines the threshold within the fuzzy class region. In the first stage of thresholding, a range of threshold values lying between  $M$  and  $N$  are obtained. In the subsequent stages, a final threshold level is picked between  $M$  and  $N$  [8]. The integral function can be represented as a function,  $y : J \rightarrow K$ , where  $J$  is a subset of  $K$ . Hence:

$$y(t) = \frac{\int_{s_1(t)}^{s_2(t)} p(u)du}{\int_{s_3(t)}^{s_4(t)} p(u)du} \tag{12}$$

where  $s_1, s_2, s_3, s_4$  are all real functions with variable  $u$  and parameters  $u_0$   $p$  is also a real function.

$$s_i : J_i \rightarrow K, J_i \subset K, \text{ and } i = 1, 2, 3, \dots$$

$$p : J_p \rightarrow K, J_p \subset K$$

For similarly spaced adjacent intervals, the integral ratio function can be expressed as:

$$y(t) = \frac{\int_t^{t_0+dt} p(u)du}{\int_{t_0+dt}^{t_0+2dt} p(u)du} \tag{13}$$

where  $t_0$  is the pivot of  $s_0$ , and  $i = 1, 2, 3, \dots$

The NIR technique determines the lower and upper bounds of the fuzzy region using estimators [8]. These estimators use the intensity histogram of the image as the threshold. Assume for example that  $q_f$  represents the intensity value of local maximum of the pixels in the foreground. Let  $q_0$  denote the background peak if it has a single background peak. Let  $q_b$  represent the background peak with the highest intensity of the background that has more than one peak.

For the lower bound of the fuzzy region,  $J$ :

$$J = q_f + \underset{t=1\dots(q_b-q_f)/2}{\operatorname{argmax}} y(t) - 1$$

where  $y(t)$  represents an NIR estimator of the form:

$$y(t) = \frac{\sum_{z_i=q_f}^{z_i=q_f+t-1} p(u_i)}{\sum_{z_i=p_f+t}^{z_i=2p_f+t-1} p(u_i)} \tag{14}$$

Additionally, for the upper bound of the fuzzy region,  $K$ :

$$K = q_f - \underset{t=1\dots(q_b-q_f)/2}{\operatorname{argmax}} y(t) + 1$$

where  $y(t)$  represents an NIR estimator of the form:

$$y(t) = \frac{\sum_{z_i=q_b}^{z_i=q_b-t+1} p(u_i)}{\sum_{z_i=p_b-t}^{z_i=p_b-2t+1} p(u_i)} \tag{15}$$

In addition,  $u_i$  represents gray-scale intensity values ranging from 0 to 255.

### 2.8. The Iterative Self-Organizing Data Analysis (ISODATA) Method

The iterative self-organizing data analysis (ISODATA) is an unsupervised classification method useful in categorizing pixels of an undefined image. The pixels for a given image are grouped into specific categories based on their spectral values [16].

Generally, in the ISODATA technique, an arbitrary threshold value is selected. Secondly, each pixel is classified according to where it falls on either side of the chosen threshold value. The mean values of each class, one class being above the threshold and the other below the threshold, are then estimated using a Gaussian distribution. Finally, the second and third steps are iterated until the change between the looping is infinitesimal [17].

### 2.9. ISODATA Algorithm

- Select an initial threshold value,  $T_0$ , for instance, half of the maximum dynamic range.
- Loop
  - Divide the histogram into two such that one segment corresponds to the foreground and the other to the background.
  - Calculate the sample mean of gray values of foreground and background pixels ( $h_f$  and  $h_m$ ).
  - Determine a new threshold value,  $T_1$ ; this is the average of these two samples' means.
  - Re-segment the histogram again into two.
- Check if any mean value has changed. If so, go to loop or else terminate.

## 3. Methodology

The proposed dynamic FFR technique calculates the optimal SINR threshold using NIR and ISOATA techniques. The frequency partitioning factor,  $\beta_{FR}$ , is set proportionately to the number of subscribers in the inner region that is based on the optimal threshold. The simulations are carried out after every 50 transmission time intervals (TTIs) to continuously update the threshold value. The results are analyzed based on edge user equipment (UE) throughput and fairness. Table 1 shows the variables used in simulations to obtain the results. The performance of the two mentioned approaches is also compared with cases where the SINR threshold is set at 5 dB and  $\beta_{FR}$  of 0.5. For each FFR configuration, UEs ranging from 10 per cell to 50 per cell are simulated. The MATLAB-based Vienna LTE-A Downlink System Level Simulator v2.0\_Q3\_2018 created by Institute of Telecommunication at Technische Universitat Wien–Vienna Austria, was used to perform the simulations [18]. For every cell, the number of user equipment per cell was continuously raised from 10 to 50 and their histograms plotted.

**Table 1.** Parameters used for the LTE FFR simulations.

Parameter	Value
UE speed	5 Km/h
Number of cells	21
UEs per cell	10, 20, 30, 40, 50
Antenna pattern	TS 36.942
Transmit power	40 W
Feedback	AMC: CQI, MIMO: RI & PMI
Shadow fading	None
Minimum-coupling loss	70 dB
Noise spectral density	−174 dBm/Hz
Simulation length	50 sub frames (TTIs)
Receiver model	Zero forcing
Inter-eNodeB distance	500
Transmission bandwidth	20 MHz (100 resource blocks)
Antennas (NTX × NRX)	4 × 2
Channel model	TU
Pathloss model	TS 36.942—Urban area, 70 dB MCL
Scheduling algorithm	Proportional fair

### System Algorithm

Table 2 illustrates the algorithm that performs the thresholding and frequency partitioning. The algorithm is first run using ISODATA. Then, the thresholding approach is substituted with NIR, and histograms and graphs are generated for each particular method.

**Table 2.** System algorithm for optimal thresholding and frequency allocation for NIR.

1. INITIATE
2. AFTER EVERY 50 TTIs DO
3. FORMULATE histogram of SINR distribution, $H_\gamma$ for UEs
4. IMPLEMENT NIR method to determine threshold, T
5. $T = \text{nirthresh}(H_\gamma)$ ; #Note: $T = \text{isothresh}$ for the case of ISODATA
6. SCALE T to $\Gamma_{th}$
7. $\Gamma_{th} = H_{\gamma_{lower\ limit}} + (H_{\gamma_{upper}} - H_{\gamma_{lower}}) \times T$
8. FFR UE MAPPING
9. PR_zone_UEs = 0
10. FR_zone_UEs = 0
11. If User Equip SINR $\geq \Gamma_{th}$
12.     ALLOT User Equip to FR zone
13.     FR_zone_UEs++
14. else
15.     ALLOT User Equip to PR zone
16.     PR_zone_UEs++
17. end
18. COMPUTE $\beta_{FR}$
19. $\beta_{FR} = \text{FR\_zone\_UEs} / (\text{FR\_zone\_UEs} + \text{PR\_zone\_UEs})$
20. SET new values of $\Gamma_{th}$ and $\beta_{FR}$

## 4. Results

The dynamic FFR threshold for NIR and ISODATA used in the simulation are shown in Tables 3 and 4, respectively. The tables also indicate the frequency-partitioning factor,  $\beta_{FR}$ .

**Table 3.** NIR parameters.

	1	2	3	4	5
Number of UEs per cell	10	20	30	40	50
Total number of UEs	210	420	630	840	1050
Optimal $\Gamma_{th}$ (dB)	4.24	3.33	3.27	0.11	3.33
$\beta_{FR}$	0.347	0.53	0.48	0.59	0.46

**Table 4.** ISODATA parameters.

	1	2	3	4	5
Number of UEs per cell	10	20	30	40	50
Total number of UEs	210	420	630	840	1050
Optimal $\Gamma_{th}$ (dB)	3.66	4.26	3.51	3.87	3.92
$\beta_{FR}$	0.34	0.33	0.40	0.36	0.35

### 4.1. UE Wideband SINR Distributions

The resultant histograms in Figures 2–6 showing the wideband SINR distributions for user equipment after 50 TTIs are represented as per Table 3. The threshold for any distribution is represented by the dotted line in the figures. The histogram shows the number of UEs with a certain SINR signal value. The horizontal scale represents the SINR value, while the vertical scale shows the numbers of UEs. In every case, the frequency partitioning parameter is also calculated. The dotted line represents the SINR threshold for the respective histograms. There are five histograms for the different cases where the cell is loaded progressively from 10 UEs per cell to 50 UEs per cell.

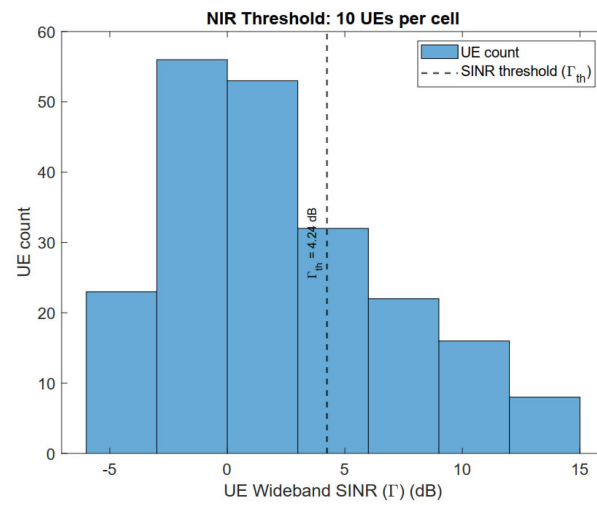


Figure 2. Wideband SINR distribution for 10 UEs.

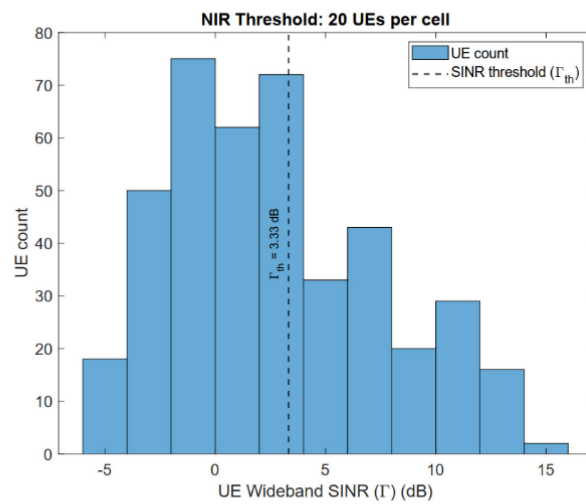


Figure 3. Wideband SINR distribution for 20 UEs.

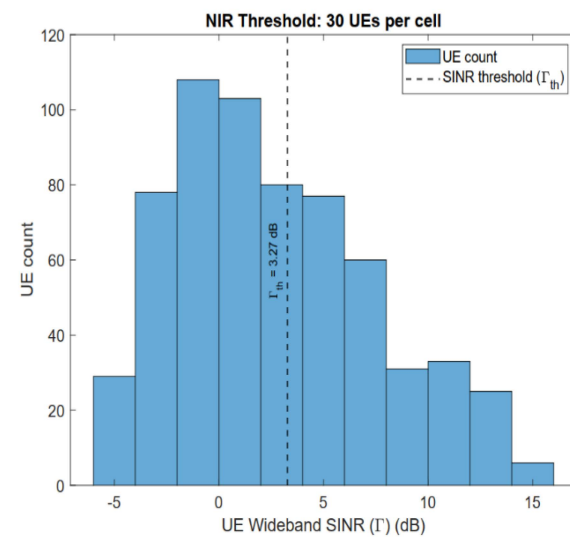


Figure 4. Wideband SINR distribution for 30 UEs.

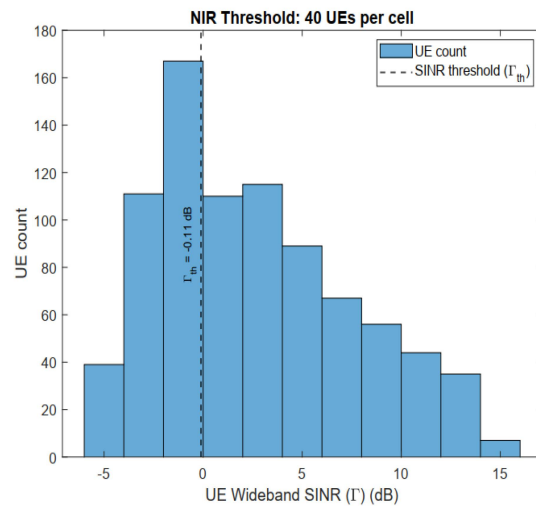


Figure 5. Wideband SINR distribution for 40 UEs.

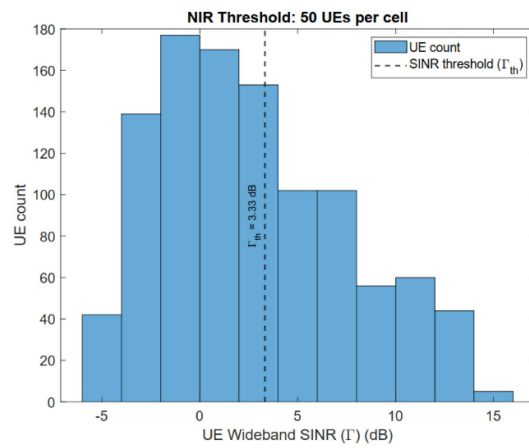


Figure 6. Wideband SINR distribution for 50 UEs.

4.2. Empirical Cumulative Distributed Function (ECDF) Curves

The ECDF curves shown in Figures 7–11 measure the probability of achieving a particular throughput. The y-axis represents the probability which ranges from 0–1, and the x-axis represents the throughput in Mbps.

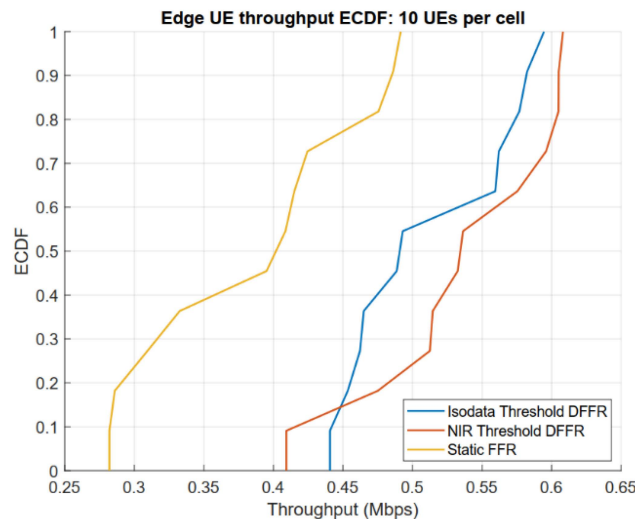


Figure 7. Edge UE throughput ECDF for 10 UEs per cell.

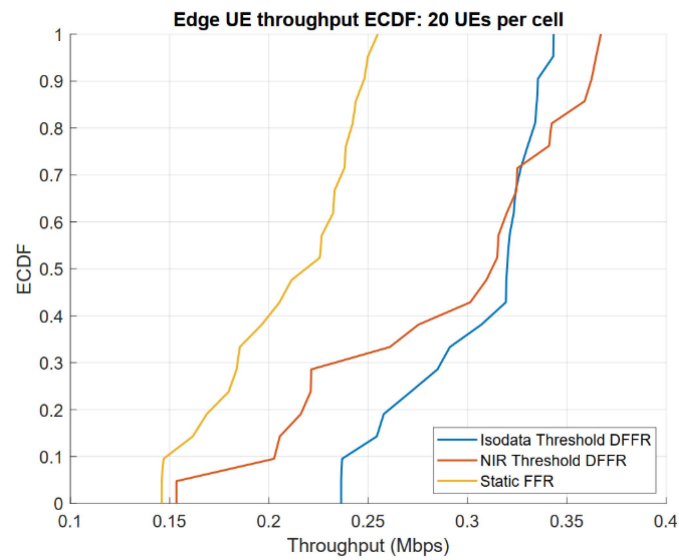


Figure 8. Edge UE throughput ECDF for 20 UEs per cell.

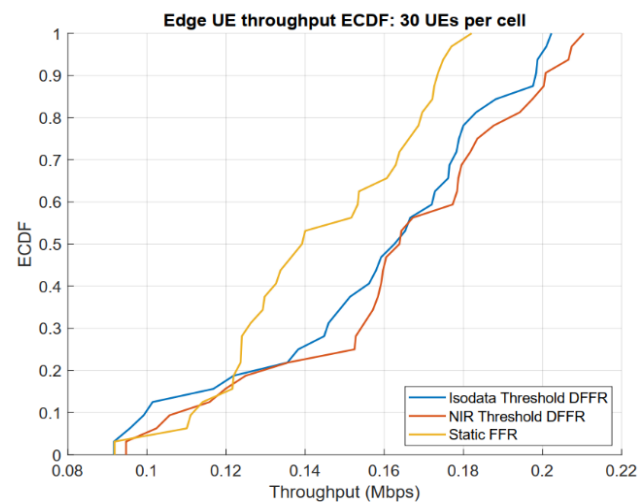


Figure 9. Edge UE throughput ECDF for 30 UEs per cell.

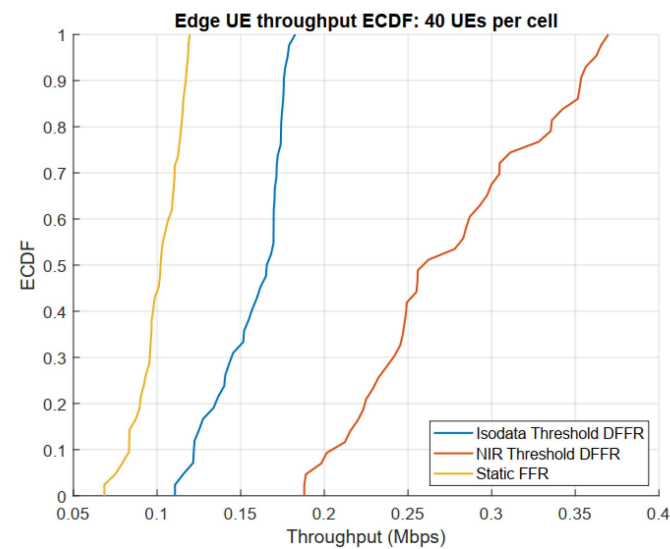


Figure 10. Edge UE throughput ECDF for 40 UEs per cell.

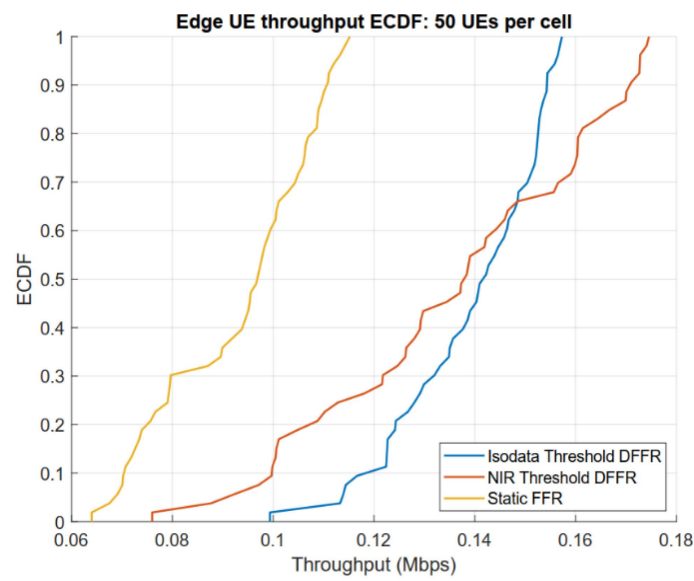


Figure 11. Edge UE throughput ECDF for 50 UEs per cell.

Figure 12 represents peak edge UE throughput; Figure 13 represents the average edge UE throughput, while Figure 14 represents the fairness metric.

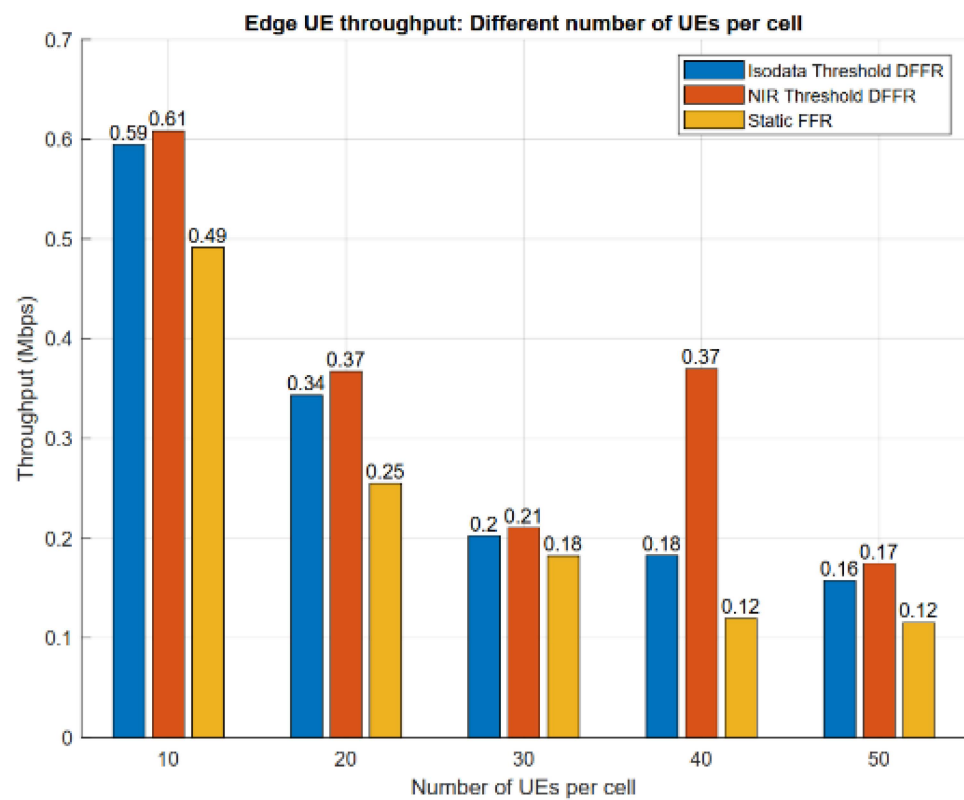


Figure 12. Peak edge throughput for a number of user equipment per cell.

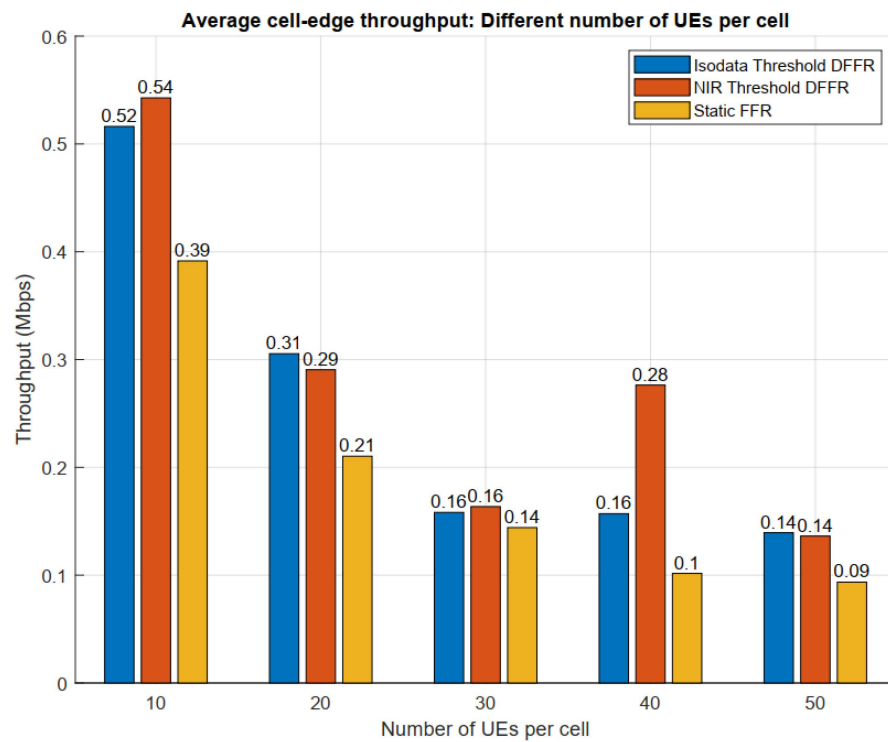


Figure 13. Average edge throughput for a number of user equipment per cell.

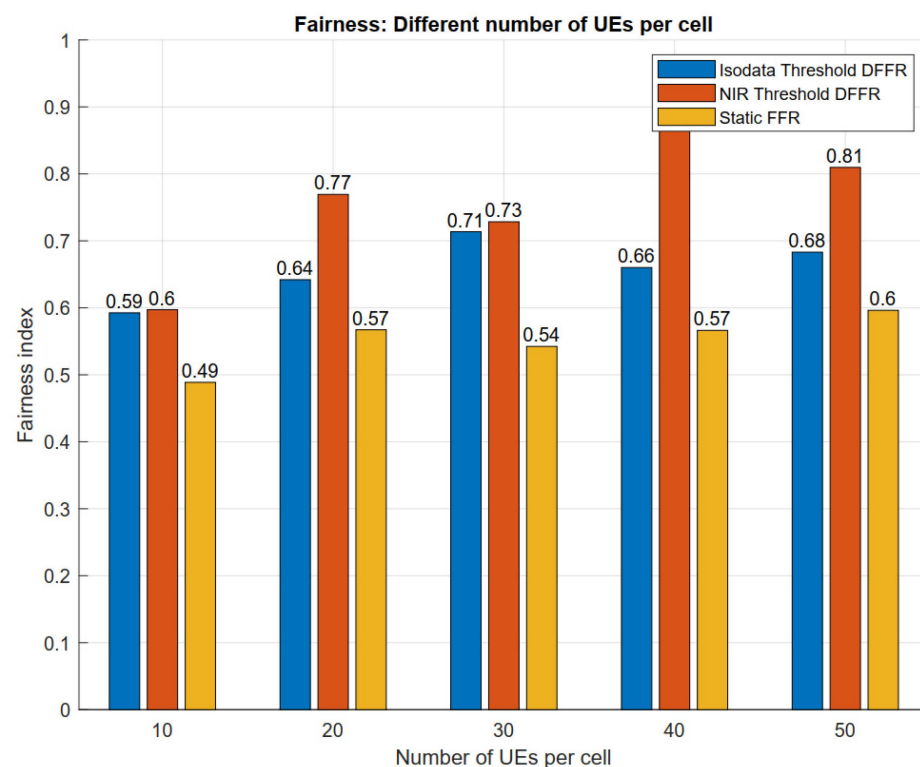


Figure 14. FFR configurations fairness chart for different number of user equipment per cell.

### 5. Discussion

The ECDF curve shows the probability of achieving a particular throughput. Consider Figure 7 where the case of 10 UEs per cell. For a throughput value of 0.5 Mbps, the probability of achieving that throughput was 0.25 for NIR or 25%, meaning 75% of UEs achieve throughputs higher than 0.5 Mbps. The performance of ISODATA at that point was

0.55 or 55%, meaning only 45% of UEs achieved throughputs higher than 0.5 Mbps. Whereas for static FFR, all the UEs fell below 0.5 Mbps, meaning the NIR method outperformed ISODATA thresholding and the static FFR approach. In some cases, such as in Figure 8, in the case of 20 UEs per cell, ISODATA outperformed NIR up to throughputs of 0.325; beyond that threshold, NIR performed better. These ECDF curves, therefore, came in handy in determining the probability of UEs achieving a certain minimum throughput level or service level. The graph in Figure 12 showed the highest individual edge UE throughput achieved by the various approaches. Figure 13 shows the graph of the average edge throughput for all the UEs for the various approaches under different cell-load conditions. Figure 14 shows the fairness graph. The higher the fairness index, the better since UEs with poor SINR were also catered for. NIR technique achieved the highest peak throughput values from 10 UEs per cell to 50 UEs per cell. For 10 UEs, 0.61 Mbps was recorded, and ISODATA recorded 0.59 Mbps while static FFR is 0.49 Mbps. This shows that NIR outperformed ISODATA by 3.3% and outperformed static FFR by 19.7%. For 50 UEs per cell NIR reported 0.17 Mbps, while ISODATA was 0.16 Mbps and static FFR was at 0.12 Mbps. NIR outperformed ISODATA by 5.9%, while it outperformed static FFR by 29.4%. Average throughput would be a more desirable measure of performance. All the edge UE figures are considered instead of a single peak value. NIR at 10 UEs per cell reported 0.54 Mbps, while ISODATA reported 0.52 Mbps and static FFR is 0.39 Mbps. NIR performed 3.7% and 27.8% better than static FFR. For 50 UEs, NIR and ISODATA performed the same at 0.14 Mbps but did better than static FFR at 0.09 Mbps. In only one instance of 20 UEs per cell, ISODATA marginally outperformed NIR by 6.5%.

## 6. Conclusions

This paper targeted to improve throughput and fairness in FFR schemes. This was achieved using global thresholding techniques, i.e., ISODATA and NIR to set the SINR threshold. The results were validated by comparing throughput and fairness of the two approaches with static FFR. Previous approaches have lacked the dynamic aspect of continuously updating the SINR threshold. Our approach periodically updated the SINR threshold after every 50 TTIs. Scheduling was done using the PF scheduler. We set up simulations using the MATLAB-based Vienna LTE system level simulator. We used scripts and functions to implement the thresholding algorithms, as shown in the methodology. We varied the number of UEs per cell to demonstrate varying cell loads. We concluded from the ECDF curves that NIR had the highest probability of achieving the best throughput for a targeted minimum network throughput value. We also concluded that NIR outperformed both ISODATA and static FFR in terms of edge throughput, as shown in Figure 12. This edge throughput represented the highest throughput achieved by a subscriber in the cell edge. We also concluded that NIR and ISODATA perform similarly when it comes to average throughput. NIR and ISODATA significantly outperformed static FFR in terms of throughput. However, when it comes to fairness, NIR consistently outperformed ISODATA and static FFR. Overall, despite ISODATA marginally outperforming NIR in average throughput in the case of 20 UEs per cell, we can conclude that NIR has superior performance. For the case of static FFR method, we opine that even if other values of SINR threshold and  $\beta_{FR}$  were set, the results would still be sub-optimal. These values would not continuously adapt to the changing cell-load conditions and fluidity or movement of the subscribers. Future work can involve considering thresholding techniques that set multiple thresholds for cases of FFR schemes that have more than two regions.

**Author Contributions:** Conceptualization, A.O. and S.M.; methodology, A.O.; software, A.O.; validation, P.K. and A.O.; formal analysis, A.O.; investigation, A.O.; resources, A.O.; data curation, A.O.; writing—original draft preparation, A.O.; writing—review and editing, A.O.; visualization, A.O.; supervision, P.K. and S.M.; project administration, A.O. All authors have read and agreed to the published version of the manuscript.

**Funding:** This research received no external funding.

**Data Availability Statement:** The data that support the findings of this study are available from the authors upon reasonable request.

**Conflicts of Interest:** The authors declare no conflict of interest.

### Nomenclature

AMC	Adaptive Modulation and Coding
BS	Base Station
ECDF	Empirical Cumulative Distribution Function
CQI	Channel Quality Indicators
FFR	Fractional Frequency Reuse
FR	Full Reuse
ISODATA	Iterative Self-Organizing Data Analysis
LTE	Long-Term Evolution
LTE-A	Long-Term Evolution—Advanced
MCL	Maximum-Coupling Loss
MIMO	Multiple Input Multiple Output
MS	Mobile Station
NIR	Native Integral Ratio
OFDMA	Orthogonal Frequency Division Multiple Access
PF	Proportionally Fair
PMI	Precoding Matrix Indicator
PR	Partial Re-use
RI	Rank Indicator
RR	Round Robin
SINR	Signal-to-Interference-plus-Noise-Ratio
TTI	Transmission Time Interval
TU	Typical Urban
UE	User Equipment

### References

1. Hamza, S.; Khalifa, S.S.; Hamza, H.S.; Elsayed, K. A survey on inter-cell interference coordination techniques in OFD-MA-based cellular networks. *IEEE Commun. Surv. Tutor.* **2013**, *15*, 1642–1670. [[CrossRef](#)]
2. Afroz, F.; Sandrasegaran, K. Interference management in LTE downlink networks. *Int. J. Wirel. Mobile Netw.* **2015**, *7*, 91–106. [[CrossRef](#)]
3. Novlan, T.D.; Ganti, R.K.; Ghosh, A.; Andrews, J.G. Analytical Evaluation of Fractional Frequency Reuse for OFDMA Cellular Networks. *IEEE Trans. Wirel. Commun.* **2011**, *10*, 4294–4305. [[CrossRef](#)]
4. Senthilkumaran, N.; Vaithegi, S. Image segmentation by using thresholding techniques for medical images. *Comput. Sci. Eng. Int. J.* **2016**, *6*, 1–13.
5. Bhargavi, K.; Jyothi, S. A survey on threshold based segmentation technique in image processing. *Int. J. Innov. Res. Dev.* **2014**, *13*, 234–239.
6. Eesa, M.; Talib, H.R. Comparison of the Methods of Image Slicing after Initial Image Processing Using the Statistical Confidence Limits. *Ann. Pure Appl. Math.* **2021**, *24*, 53–64.
7. Leedham, G.; Varma, S.; Patankar, A.; Govindaraju, V. Separating text and background in degraded document images—A comparison of global thresholding techniques for multi-stage thresholding. In Proceedings of the Eighth International Workshop on Frontiers in Handwriting Recognition (IWFHR'02), Niagara-on-the-Lake, ON, Canada, 6–8 August 2002; IEEE: Piscataway, NJ, USA, 2002; pp. 244–249. [[CrossRef](#)]
8. Solihin, Y.; Leedham, G. Integral ratio: A new class of global thresholding techniques for handwriting images. *IEEE Trans. Pattern Anal. Mach. Intell.* **1999**, *21*, 761–768. [[CrossRef](#)]
9. Mapay, T.; Viriri, S.; Tapamo, J.R. Comparative study of retinal vessel segmentation based on global thresholding techniques. *Comput. Math. Methods Med.* **2015**, *2015*, 895267. [[CrossRef](#)] [[PubMed](#)]
10. Ali, H.S.; Leung, V.C. Dynamic frequency allocation in fractional frequency reused OFDMA networks. *IEEE Trans. Wirel. Commun.* **2009**, *8*, 4286–4295. [[CrossRef](#)]
11. AlAmmour, J.; Andrews, G.; Baccelli, F. SINR and throughput of dense cellular networks with stretched exponential path loss. *IEEE Trans. Wirel. Commun.* **2017**, *17*, 1147–1160. [[CrossRef](#)]
12. Basilashvili, G. Study of spectral efficiency for LTE network. *Acad. Sci. Res. J. Eng. Technol. Sci.* **2017**, *29*, 21–32.
13. Jain, R.K.; Chiu, D.M.; Hawe, W.R. *A Quantitative Measure of Fairness and Discrimination*; Eastern Research Laboratory, Digital Equipment Corporation: Hudson, MA, USA, 1984; p. 21.

14. Kim, H.; Kim, K.; Han, Y.; Yun, S. A proportional fair scheduling for multicarrier transmission systems. *IEEE Commun. Lett.* **2005**, *210–212*. [[CrossRef](#)]
15. Jawahar, C.; Biswas, P.; Ray, A. Investigations on fuzzy thresholding based on fuzzy clustering. *Pattern Recognit.* **1997**, *30*, 1605–1613. [[CrossRef](#)]
16. Vimala, R.; Marimuthu, A.; Venkateswaran, S.; Poongodi, R. Unsupervised ISODATA algorithm classification used in the landsat image for predicting the expansion of Salem urban, Tamil, Nadu. *Indian J. Sci. Technol.* **2020**, *13*, 1619–1629.
17. Ahmed, S. Comparison of Satellite Images Classification Techniques using Landsat-8 Data for Land Cover Extraction. *Int. J. Intell. Comput. Inf. Sci.* **2021**, *21*, 29–43. [[CrossRef](#)]
18. Thieu, Q.-T.; Hsieh, H.-Y.; Wang, C.-H. A Wideband Scheduling Method for Non-Orthogonal Multiple Access in the Vienna LTE-A Downlink System-Level Simulator. In Proceedings of the IEEE Globecom Workshops (GC Wkshps), Washington, DC, USA, 4–8 December 2016; pp. 1–6. [[CrossRef](#)]